

Smart Manufacturing and Material Processing (SMMP)

DOI: http://doi.org/10.26480/smmp.01.2023.41.47





RESEARCH ARTICLE

NUMERICAL STUDY ON IMPACT PERFORMANCE OF PHOSPHOGYPSUM FOAM CONCRETE

Baochun Yanga, Longfan Pengb, Hepeng Zhangc, Tianshu Chuc, Xuejun Jiab, Xiaoyang Xub, Naveed Ullah Kaka Kheld

- ^a Central & Southern China Municipal Engineering Design and Research Institute Co.Ltd, Wuhan, China
- b China Construction Second Engineering Burea Co. Ltd, Wuhan, China
- ^c Wuhan University of Technology, Wuhan, China
- ^d Mechanical Engineering Department, University of Engineering and Technology, Peshawar, Pakistan
- *Corresponding Author Email: ZH1450784300@163.com

This is an open access article distributed under the Creative Commons Attribution License CC BY 4.0, which permits unrestricted use, distribution, and reproduction in any medium, provided the original work is properly cited.

ARTICLE DETAILS

Article History:

Received 20 January 2024 Revised 18 February 2024 Accepted 11 March 2024 Available online 13 March 2024

ABSTRACT

To mitigate environmental pollution and address the issue of solid waste phosphogypsum materials, cement is utilized as a binding agent alongside various building materials to create Phosphogypsum Foam Concrete(PFC), commonly used in construction. This study focuses on the use of PFC infilled walls as the subject of investigation. The general finite element software ABAQUS was utilized to select the optimal plastic damage and elastoplastic constitutive models for concrete and reinforcement, respectively. A physical model of a 400mm*400mm*20mm PFC slab was established, and an impact load was applied to it via four-sided consolidation. By numerically studying the response of concrete under impact, by altering its strength, reinforcement ratio, and impact speed, and qualitatively analyzing the impact load, deformation, and energy dissipation of various parameter variables, a theoretical basis for the optimization and design method of PFC infilled wall is provided.

KEYWORDS

 $PFC, finite\ element\ analysis, strength\ of\ PFC, reinforcement\ ratio, impact\ response$

1. Introduction

Phosphorus fertilizers utilized in agricultural development produce phosphogypsum. The unregulated discharge and buildup of phosphogypsum significantly impairs the environment, polluting groundwater resources and leading to wastage of land resources. Consequently, it is imperative to efficiently utilize phosphogypsum as a resource. Phosphogypsum and natural gypsum possess almost identical compositions. Replacing some cement with phosphogypsum can effectively reduce carbon dioxide emissions, thus aiding in the building materials industry's goal to reach carbon peak as soon as possible (Chernysh et al., 2021; Meskini et al., 2021; Amrani et al., 2020; Pliaka and Gaidajis, 2022). Research in China has found that phosphogypsum can replace between 10% and 50% of cement content to produce lightweight foam concrete, using existing technology for the comprehensive utilization of phosphogypsum resources (Calderon-Morales et al., 2021; Li et al., 2022; Xiantao et al., 2023). This lightweight material offers excellent sound insulation and superior resistance against cracking, earthquakes, and water damage.

It can be utilized not only as filling material for different engineering foundations and prefabricated wall panels but also as a substitute for block bricks in cast-in-place non-load-bearing walls. Even though these components are not the primary load-bearing components, they can still be affected by internal objects such as furniture, people, and equipment during structural vibrations and deformations. This can cause damage or destruction to the walls and even lead to collapse and accidents. The impact response of Phosphogypsum Foam Concrete (PFC) material deserves discussion and study to guarantee the safety of the structure and personnel under accidental loads.

Recently, the response of materials and components to low-speed impact has garnered much attention in academic research. Collisions between structures or components and other objects during normal operation can cause damage or even result in material and structural failure. Thus, scholars have investigated the impact performance of traditional building materials, such as concrete and its components. A group researcher conducted impact tests on a set of high-performance concrete slabs (Dancygier et al., 2007). The experimental findings revealed that the impact resistance of structures and components is not solely determined by the strength of concrete, but rather by various factors that must be considered comprehensively. Zineddin conducted dynamic response analyses of reinforced concrete plates subjected to impact loads through drop hammer impact tests, examining three different reinforcement methodologies (Zineddin and Krauthamner, 2007). ABAQUS was utilized to simulate the testing process.

The results of both the test and simulation analysis indicate that the reinforcement method and ratio predominantly controlled the failure mode of the test plate under impact loads. Hamid Sadraie et al. performed drop hammer impact tests on reinforced concrete slabs utilizing GRFP and carried out numerical simulations on the specimen model using the finite element method (Sadraie et al., 2019). The examination determined that when impacted, GFRP reinforced concrete slabs had larger crack areas. However, by optimizing the reinforcement ratio and GFRP bar arrangement, the slabs perform better than reinforced concrete slabs. A group researchers utilized a pendulum device to conduct impact tests on ordinary concrete and high-strength concrete GFRP reinforced columns with varying reinforcement ratios (Pham et al., 2021).

Quick Response Code Access this article online



Website:Website: www.topicsonchemeng.org.my

DOI:

10.26480/smmp.01.2023.41.47

The study demonstrated that the longitudinal reinforcement ratio of GFRP bars had a greater effect on the column's failure mode and impact resistance compared to concrete strength. Tabatabaei et al. conducted a comparative study on the impact resistance of plain concrete, reinforced concrete, and carbon fiber reinforced concrete slabs (Tabatabaei and Voir, 2014). Their findings revealed that the addition of 1.5% carbon fiber content can enhance the impact resistance of concrete slabs, reducing the degree of fragmentation under impact by approximately 90%. Liu et al. carried out drop hammer impact tests on concrete beams mixed with short cut carbon fiber, steel fiber, and glass fiber (Liu et al., 2018). The study demonstrated that the bending toughness of concrete reinforced with carbon fiber and glass fiber increased with higher impact speed and dosage.

Additionally, the peak impact force of concrete containing short cut steel fibers was found to be greater. A group researchers conducted tests to ascertain the mechanical properties of C50 concrete using a proprietary drop hammer testing apparatus, revealing the cumulative damage effects of low-speed impact on C50 and analyzing C50 concrete's evolution of damage under such conditions (Lei et al., 2020). Ye conducted drop and pendulum tests to examine the response of concrete under various angles of amplified impact loads (Ye et al., 2023). Their findings suggest that amplified impact decreases the energy absorption capacity of concrete targets and increases their failure rate. In another study, Cai investigated the effects of impact load and velocity on the response and failure mechanism of reinforced concrete beams subjected to dynamic loads (Cai et al., 2017; Gong, 2023). The research findings reveal that the inertia effect exerted by concrete significantly influences the impact resistance of reinforced concrete beams.

To analyze the response of PFC to impact, this paper utilizes the finite element software, ABAQUS, to conduct a numerical analysis of PFC and concrete slab. The impact simulation of PFC slab was performed by varying variables as the concrete strength and reinforcement within the concrete slab. The simulation applied suitable boundary conditions and material constitutive laws to enable a qualitative comparative analysis of the response of PFC slabs under impact loads.

2. PREPARATION OF PFC

2.1 Mix Proportion of PFC

The gray powder solid phosphogypsum used in this experiment is displayed in Figure 1. It has a determined density of 2.73 g/cm3. The fly ash used is principally comprised of SiO2 and Al2O3, with volcanic ash properties, and has a density of 2.33 g/cm3. It can be used as a concrete admixture. The cement utilized is P.O42.5 Portland cement, a hydraulic cementitious material produced from Portland cement clinker, 6%-20% mixed material, and a finely ground appropriate amount of gypsum. And all performance indicators meet the applicable provisions stated in the "Portland Cement" standard (GB175-2007).



Figure 1: Phosphogypsum solid powder

The mix design for each component of the tested cement mortar follows the Test Specification for Polymer Modified Cement Mortar, which prescribes a mass ratio of cement to sand between 1:1.5-1:2. The mix ratio for PFC mortar in this study is as follows: water-cement ratio of 0.5, 200g of water, 360g of cement, 40g of phosphogypsum, 10g of phosphogypsum dosage, and 800g of sand. Weigh the necessary raw materials and a specified quantity of water according to the given design mix ratio. Dissolve the activator in water and mix it with the materials, stirring until the mixture is even. Load the mixed substance into a mold and compress it on a concrete compaction table. After 24 hours, remove the mold and place the formed specimens in a standard curing box for curing. Take out the specimens after 28 days of curing, and determine the strength of the resulting PFC, which is 10MPa.

2.2 Preparation Technology of PFC

According to the Technical Specification for PFC Partitions and Filling Materials, in compliance with the local standards of Hubei Province, the initial task involves accurately measuring and evenly mixing different ingredients. Subsequently, the phosphogypsum, cement, lime, and other powders are dry-mixed in a mixer for a minute followed by the addition of the metered admixture. The mixture is then combined with water and mixed for four minutes. The second step entails utilizing a foam agent to prepare foam. A high-speed mixer is utilized to combine the foaming agent and water in a 1:20 mass ratio for 3-5 minutes, until a uniform foam is achieved. It is vital that there is no leftover foaming agent solution in the mixing bucket to complete the foam preparation. The third step involves evenly mixing the foam with the mixed slurry to produce PFC. The foam concrete should be quickly poured into a pre-oiled mold and covered with a layer of preservative film to prevent collapse due to moisture loss. Place the sample indoors for 24 hours and remove the mold after it has fully hardened naturally. Then, mark and place the foam concrete test block in the standard curing room for 28 days before conducting the subsequent test. Please refer to Figure 2 for the appearance of PFC, and Figure 3 for its preparation process.



Figure 2: Phosphogypsum foam concrete

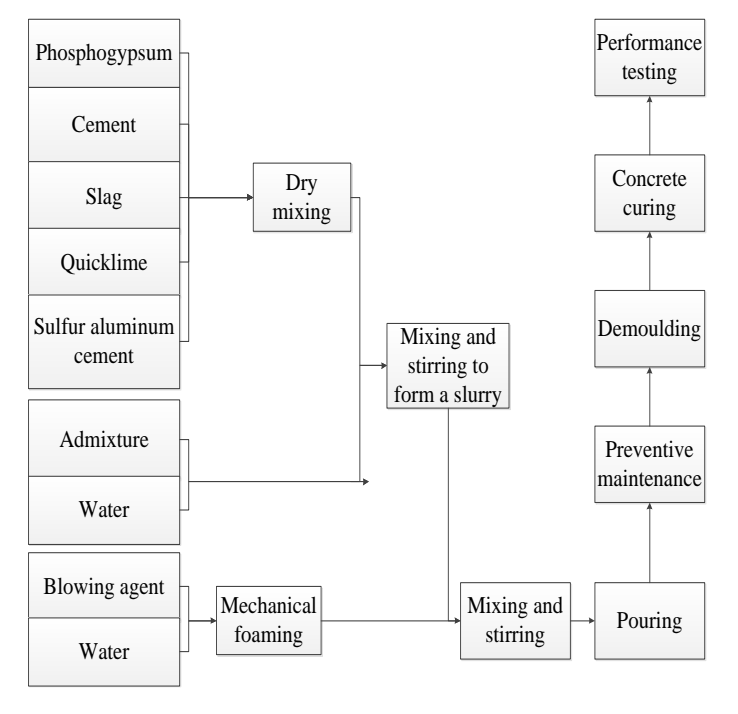


Figure 3: Preparation Process of PFC

3. LOW SPEED IMPACT FINITE ELEMENT ANALYSIS

3.1 Finite Element Theory

Based on the finite element theory and real-life situation, this paper utilizes the finite element software ABAQUS to conduct numerical modeling of PFC slabs. Furthermore, the impact response of the PFC is simulated and analyzed by selecting suitable constraint conditions and material composition. The detailed modeling process and parameter selection are presented below.

3.2 Material Parameters and Material Models

3.2.1 Material Parameters

The performance parameters of PFC, regular concrete, and steel used in this model were all tested and are presented in Table 1 (Peng et al., 2023).

Table 1: Material parameters										
	Elastic modulus (GPa)	Yield strength (MPa)	Ultimate strength (MPa)	Ultimate strain	Poisson's ratio	Density (g/cm ³)				
Ordinary Concrete	36.4		50	3678	0.2	2400				
PFC	10		10	3678	0.2	1044				
Rebar	190	435	683	40000	0.3	7800				

3.2.2 Constitutive Model of Concrete

Due to the intricate composition and discrete behavior of concrete materials, a universally acknowledged material model does not exist at present. Rather, constitutive models of concrete materials predominantly rely on experimental induction or semi-theoretical and semi-empirical methods.

The concrete constitutive model, as specified in the "Code for Design of Concrete Structures" (GB50010-2010) and illustrated in Figure 4, is primarily suited for design purposes (citing a literature). There is no mention of strength alterations in concrete following damage.

ABAQUS offers models for brittle cracking, dispersion cracking, and plastic damage in concrete materials (Li et al., 2023). Since the plastic damage model applies directly to the two-dimensional stress state by defining the concrete shear modulus transfer coefficient and damage parameters and has few parameters and easy convergence, the stress-strain curve obtained from the test agrees well with the model, as noted in the article's specification and report (Peng et al., 2023). This study employs the concrete plastic damage model to conduct low-speed impact simulation calculations on C50 concrete slabs and PFC slabs. The uniaxial compressive constitutive model formulation is presented in the equation (1), and the resulting stress-strain curve of compressed concrete is illustrated in Figure 5 (Li et al., 2023).

$$\sigma_{c} = \begin{cases} f_{c} \left[2(\varepsilon_{c} / \varepsilon_{c0}) - (\varepsilon_{c} / \varepsilon_{c0})^{2} \right] & (0 \leq \varepsilon_{c} \leq \varepsilon_{c0}) \\ f_{c} \left[1 - 0.15 \left(\frac{\varepsilon_{c} - \varepsilon_{c0}}{\varepsilon_{cu} - \varepsilon_{c0}} \right) \right] & (\varepsilon_{c0} < \varepsilon_{c} \leq \varepsilon_{cu}) \end{cases}$$
(1)

In the equation (1), fc is taken as the standard value of 0 degrees of concrete axial compressive strength; take 0.002 as c0.

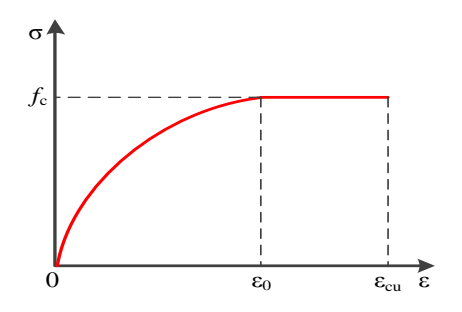


Figure 4: Concrete stress-strain curve in design specifications

The uniaxial tensile stress-strain model of concrete is determined by the formula recommended in Appendix C of the "Code for Design of Concrete Structures", and the specific expression is shown in the equation (2).

$$\sigma \begin{cases} f_{t}[1.2(\varepsilon_{t}/\varepsilon_{t0}) - 0.2(\varepsilon_{t}/\varepsilon_{t0})^{6}] & (0 \leq \varepsilon_{t} \leq \varepsilon_{t0}) \\ f_{t} \frac{(\varepsilon_{t}/\varepsilon_{t0})}{\alpha_{t}((\varepsilon_{t}/\varepsilon_{t0}) - 1)^{1.7} + (\varepsilon_{t}/\varepsilon_{t0})} & (\varepsilon_{t0} < \varepsilon_{t} \leq \varepsilon_{tu}) \end{cases}$$

$$(2)$$

In the equation (2), ft is taken as the standard value of the axial tensile strength of concrete; t0 is calculated from the equation t0=ft/Ec, taking 0.000085; t is the parameter value of the descent segment, which is taken as 2.96 by linear interpolation. The calculated tensile stress-strain curve of concrete is shown in Figure 6 (Li et al., 2023).

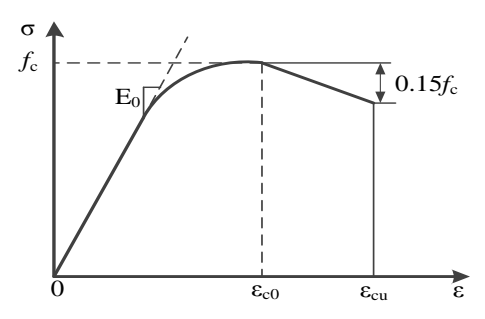


Figure 5: Compression stress-strain curve of concrete

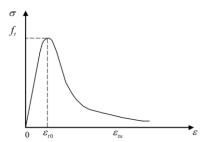


Figure 6: Tensile stress-strain curve of concrete

The main related parameter values of the concrete model are shown in Table 2.

Table 1: Relevant parameters of the concrete plastic damage model								
Expansion angle(°)	Offset	b ₀ /c ₀	$K_{\rm c}$	Viscosity coefficient				
32	0.1	1.16	0.6667	0.001				

3.2.3 Steel Bar Constitutive Model

Steel reinforcing bar's constitutive model primarily utilizes the ideal elastic-plastic model, as illustrated in Figure 7 (Wang, 2023). Equation (3) exemplifies the constitutive equation.

$$\sigma = \begin{cases} f_y & \varepsilon > \varepsilon_y \\ E_s \varepsilon & \varepsilon \le \varepsilon_y \end{cases} \tag{3}$$

In the equation (3): Es represents the elastic modulus of the steel, ϵy refers to the yield strain of the steel, and fy denotes the yield strength of the steel.

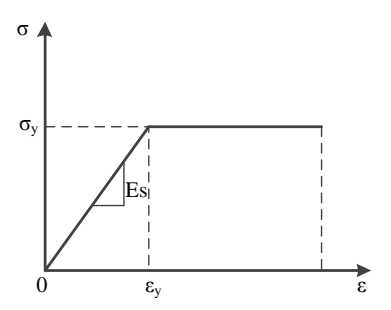


Figure 7: Ideal elastoplastic model of steel reinforcement

3.3 Establishment of Finite Element Model

3.3.1 Create Components and Assemblies

In this paper, a three-dimensional model of PFC slabs are established using a solid element structure in a finite element model. The hammer head's rigidity, due to its make of die steel, allows for the omission of resulting deformations. Thus, discrete rigid bodies simulate the hammer head. The concrete slab measures 400mm*400mm*20mm and is uniformly reinforced with 4*4 @ 100 steel mesh structure, each with a 50mm protective layer thickness. The arrangement of the concrete slab model and the reinforcement mesh in the PFC can be seen in Figure 8.

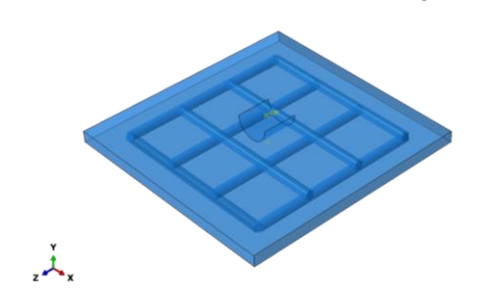


Figure 8: Component layout

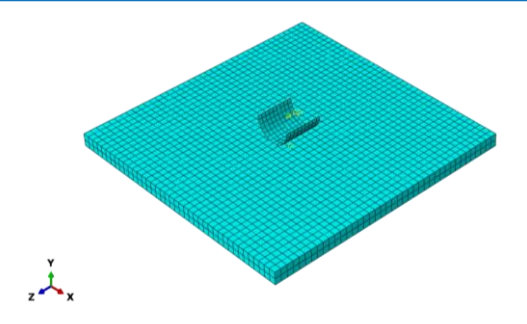


Figure 9: Grid division diagram

3.3.2 Grid Division

After considering the mesh convergence of the finite element mode, and the efficiency and accuracy, optimal mesh scheme were selceted and illustrated in Figure 9. Divide the head of the hammer into 126 units, and assign discrete rigid bodies as the unit attributes. Divide the concrete slab into 3200 units, and choose three-dimensional stress as the unit attribute. Finally, turn on the unit deletion option to observe the concrete slab's damage after the impact. Each steel bar within the steel mesh should be divided into 50 units, and the truss set as the unit attribute.

3.3.3 Interaction and Boundary Conditions

The PFC slab and the hammer head in the finite element model utilize the general contact type. Due to a lack of friction consideration, the contact property's tangential behavior is specified as zero friction, and the normal behavior is set to hard contact. The interaction module establishes rigid body constraints on the hammer head and joins the steel mesh and concrete slab with built-in areas.

Given that this experiment solely necessitates the vertical movement of the hammer head, the remaining 5 degrees of freedom pertaining to the impact hammer head can be completely restrained, with the exception of the impact direction. In addition, the concrete slab's surrounding regions can be entirely fixed to permit only movement in the impact direction. The model's boundary conditions are presented in Figure 10.

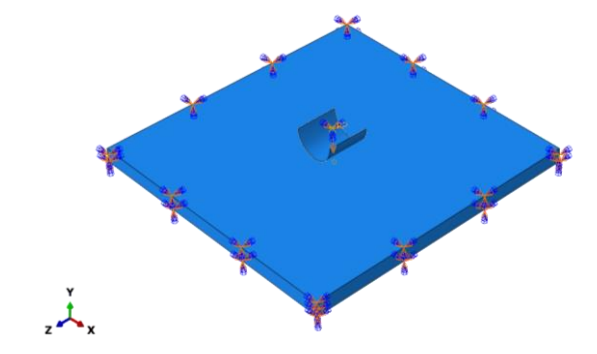


Figure 10: Schematic diagram of boundary conditions

4. RESULT ANALYSIS AND DISCUSSION

4.1 The Influence of Concrete Strength on Impact Response

To analyze the effect of concrete strength on the impact performance and damage, we compared the impact response of concrete with an ultimate compressive strength of 50MPa and a PFC slab with an ultimate compressive strength of 10MPa. Both were tested under fixed support on all sides and no reinforcement mesh, with an impact speed of 25m/s.

The failure modes of the plate under different conditions, obtained from an analysis using finite element models, are depicted in Figure 11. The stress cloud map of the C50 concrete slab is presented in Figure 11(a) (b), which reveal the formation of only irregular cracks as there is no complete penetration of the slab, and stress concentration at its bottom. Figure 11(c) (d) showcase the stress nephogram of the PFC slab. The slab has been fully penetrated, and the highest stress levels are concentrated in the area surrounding the opening created by the hammer head.

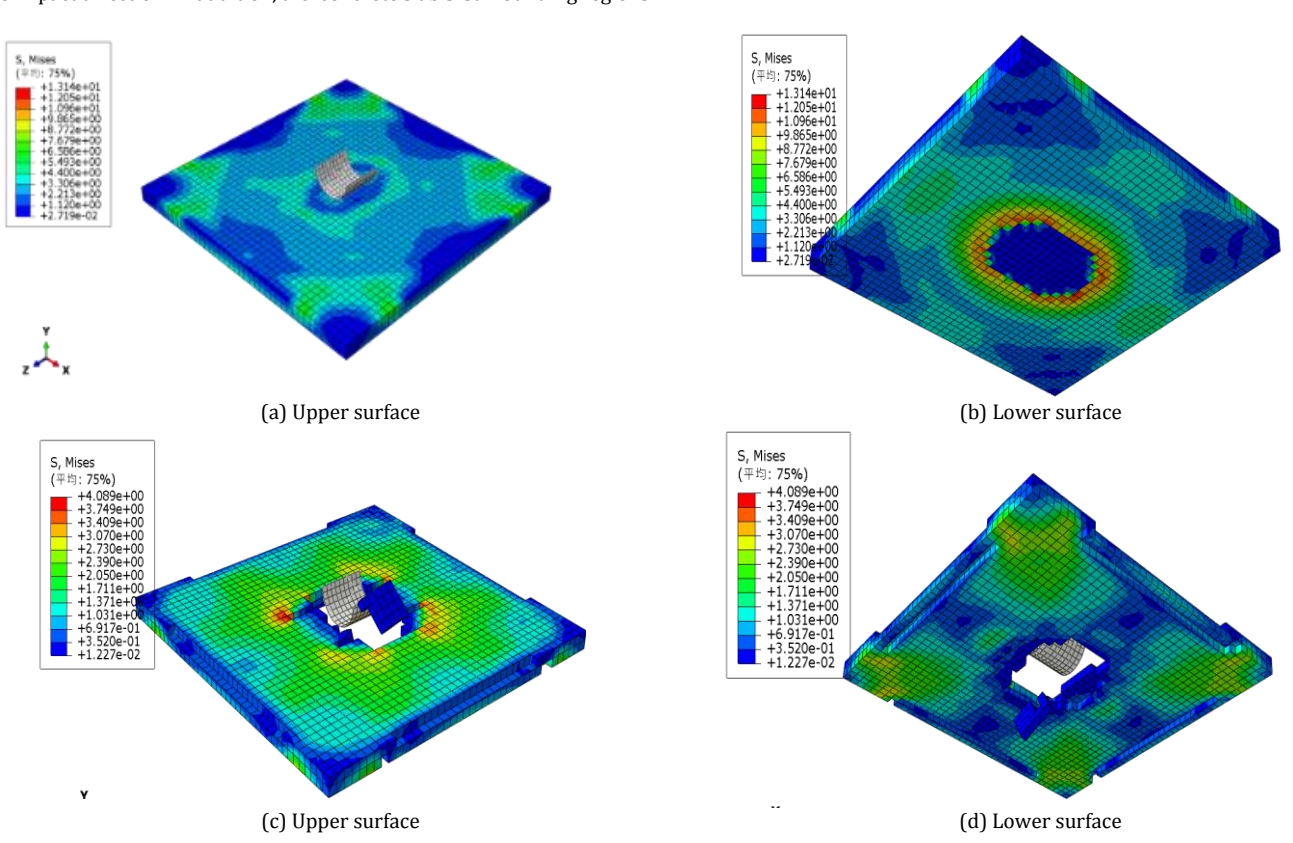


Figure 11: The damage to both C50 concrete slab (a) and (b) and PFC (c) and (d)

The time impact curve for C50 and PFC are displayed in Figure 12. As loading commences, the specimen's impact force linearly rises over time. Following the force surpassing the initial threshold, the plate's stiffness modifies due to damage, resulting in a turning point in the curve. The impact force decreases rapidly until it reaches zero. Upon comparing the two specimens, it was discovered that the peak impact load of C50 concrete slab is approximately four times that of PFC slab, while the strength differs

only five times. This finding suggests that the strength of concrete does not correspond one-to-one with the impact load during low-speed impact. Furthermore, the impact load time curve of the C50 concrete slab began to fluctuate at 59ms due to the lack of perforation in the specimen, as depicted in Figure 11 (a)(b). It was at this point when the hammer head commenced rebounding, and the impact force gradually dissipated to zero.

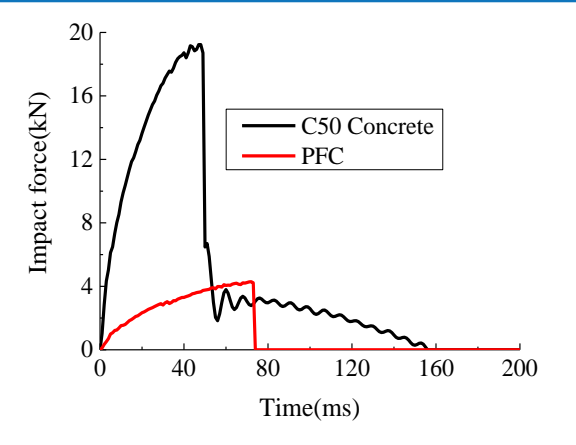


Figure 12: Impact force time curve

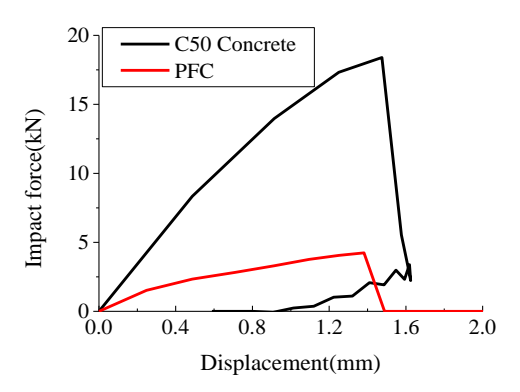


Figure 13: Impact force displacement curve

The impact force displacement curves of the two types of specimens are shown in Figure 13, and it is not difficult to find that their curves can be roughly divided into two stages: First, from loading to damage reaching the damage threshold; Subsequently, the specimen underwent fracture damage, and the impact load rapidly decreased with displacement until it reached 0. In addition, the peak displacement corresponding to the peak force of C50 concrete slab and PFC slab is 1.57mm and 1.38mm

respectively. Due to the perforation failure of the PFC slab as shown in Figure 11 (c) (d), its descending section is significantly convex, while the C50 concrete slab is locally damaged, and its descending section of the impact load displacement curve is concave.

Figure 14 displays the ultimate energy value that represents the complete energy dissipation of the specimen. The correlation between the strength of the specimen and the dissipated energy is evident. The energy peak of the 50MPa strength concrete slab is approximately 8 times higher than that of the PFC slab. This finding suggests that the PFC slab has perforation damage, although other damage is not apparent, while the C50 concrete slab only has small, local damage. Increasing the concrete's strength can enhance its energy absorption capacity. Furthermore, the two types of specimens display divergent peak energy attainment times, which decrease with higher strength. This disparity can be attributed to dissimilar plastic deformation abilities that arise from strength variations, which in turn directly impact the hammer head's acceleration.

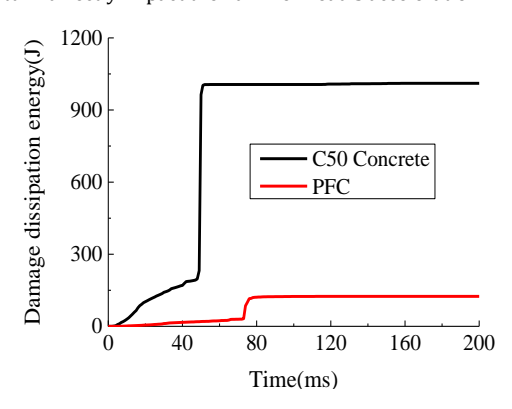
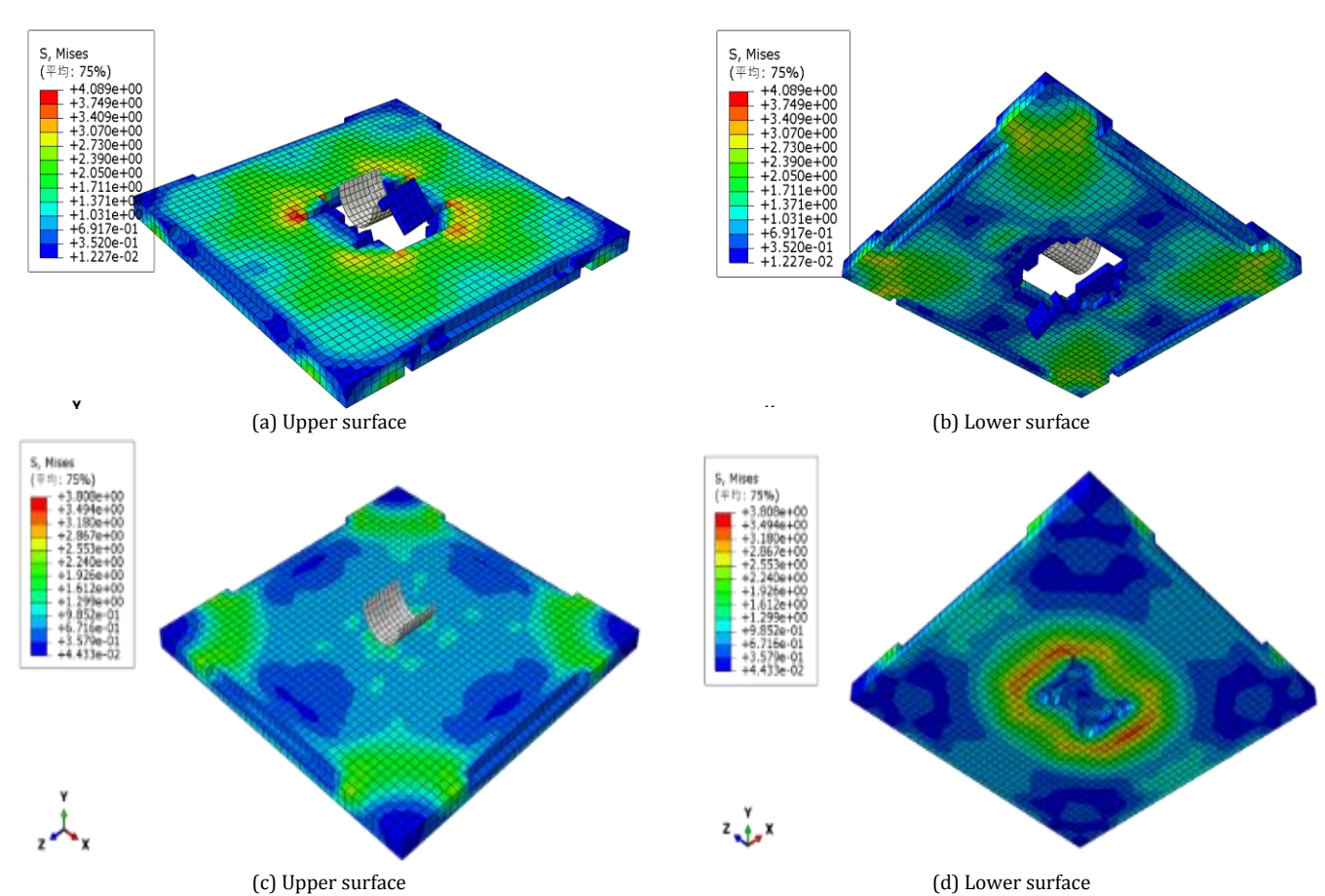


Figure 14: Damage dissipation energy time curve

4.2 Effect Of Reinforcement on Impact Response

To examine the dynamic response of PFC to low-speed impact at varying reinforcement ratios, the impact speed was set to 25m/s with constant constraint conditions. Reinforcement diameters of 0mm, 8mm, 16mm, and 24mm were selected. A comparative analysis of the low-speed impact properties of PFC slabs was performed based on finite element numerical simulation results.



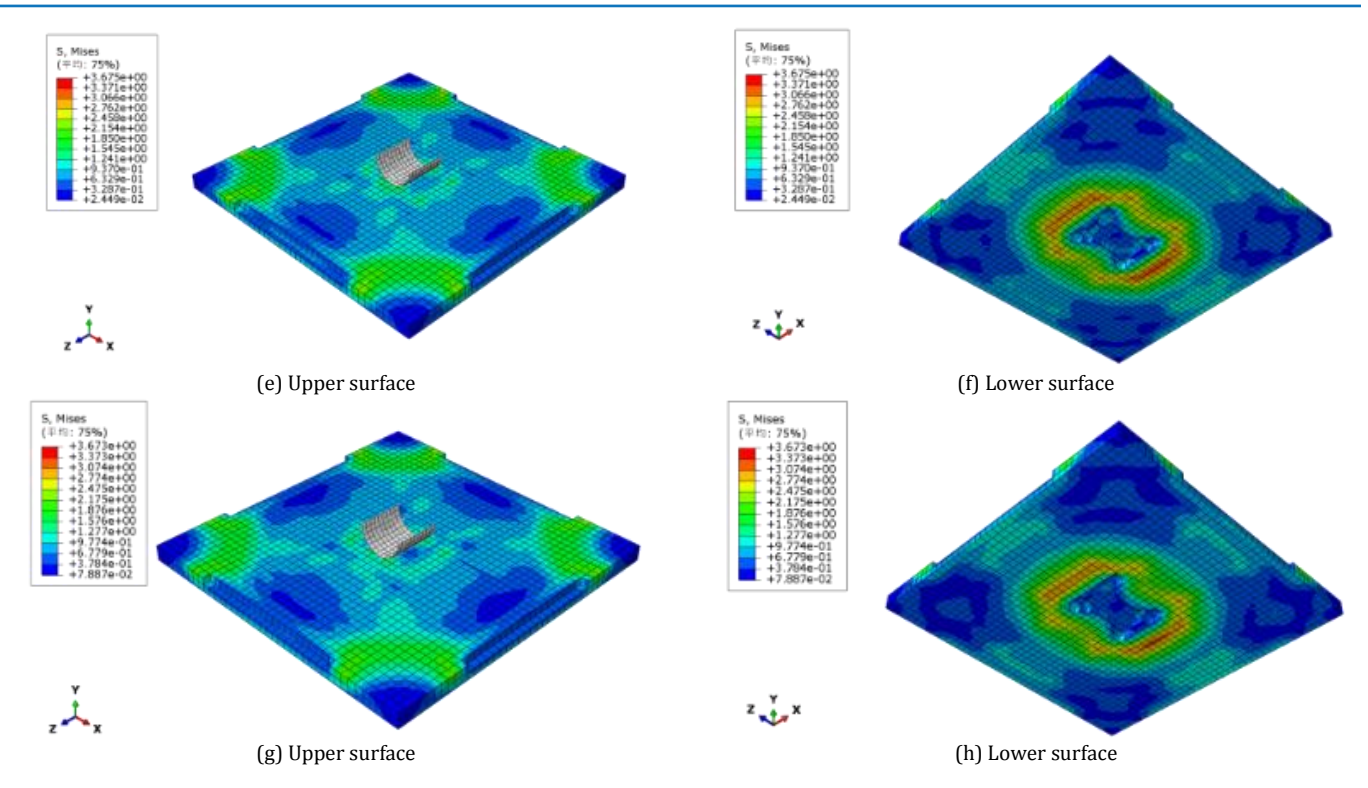


Figure 15: Damage caused by low-speed impact on steel bars with various diameters

The time curve of the impact force is displayed in Figure 16. Post reaching its threshold at approximately 73ms, the impact load resulted in a change in stiffness, leading to a turning point on the curve and causing the load to rapidly decrease, due to the specimen without reinforcement's perforation failure as shown in Figure 15 (a) (b). Though the reinforced specimen was not perforated, its bottom suffered damage and reached the threshold at around 102ms. The curve exhibited a point of inflection and the base sustained damage, leading to a reduction in load. Compared to the peak impact load, the peak impact load of PFC slab with reinforcement diameters of 8mm, 16mm, and 24mm is nearly identical, but it is 15.2% higher than that of the slab without reinforcement. Adding reinforcement can enhance the peak impact load of PFC specimens; However, its value is insignificantly related to reinforcement diameter.

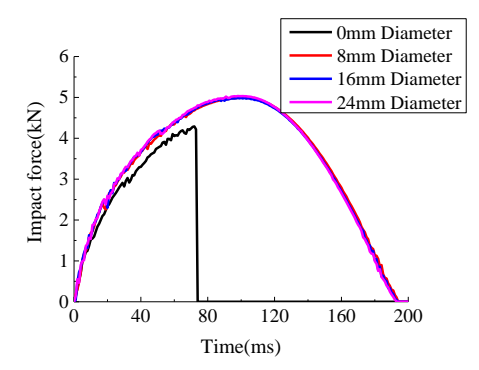


Figure 16: Impact force time curve

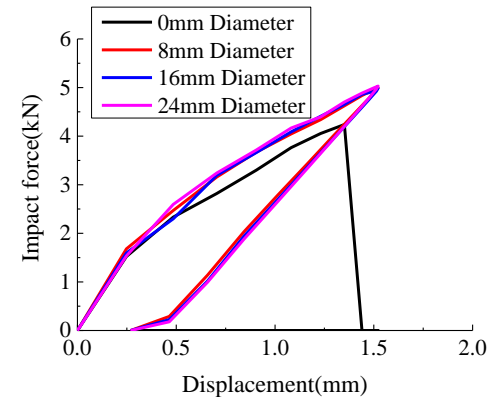


Figure 17: Impact force displacement curve

The impact displacement curves for four different reinforcement diameters are illustrated in Figure 17. The PFC slab showed a perforation displacement of 1.45mm without reinforcement, while the same slab with reinforcement exhibited a residual displacement of approximately 0.27mm. This outcome suggests that the reinforcement composite effectively enhances the plastic deformation capacity of the tested specimen. The specimen lacking reinforcement was penetrated, and the descending portion of the displacement curve for the impact force is notably convex. Conversely, the reinforced specimen was not penetrated, but the bottom was damaged, as depicted in Figure 15 (c) (d) (e) (f) (g) (h). The descending portion of the displacement curve for the impact load is concave.

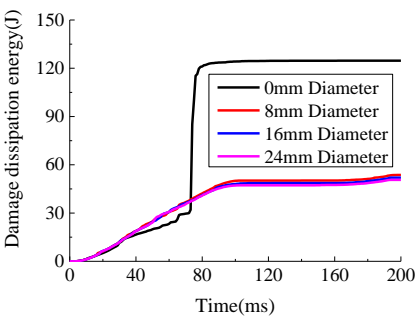


Figure 18: Damage dissipation energy time curve

Figure 18 displays the time-energy curves for damage dissipation of four specimen groups with varying reinforcement ratios. The PFC slab without reinforcement exhibits perforation failure. In Figure 18, the dissipation energy of damage sharply increased at approximately 73 milliseconds and then stabilized. The other three groups of PFC slabs with reinforcement only experienced bottom failure without perforation, and the curve of damage dissipation energy increasing with time was comparatively gradual. The peak energy of the PFC slab but without reinforcement is roughly 2.4 times greater than that of the one with reinforcement. Furthermore, the failure modes remain consistent across three groups of specimens of varying diameters, with no significant change in absorbed energy as steel bar diameter increases. These results suggest that the diameter of the steel bar has little impact on its energy absorption capacity.

5. CONCLUSION

This study examines the response of PFC to impacts. The responses of unreinforced PFC and C50 concrete to an impact speed of 25m/s are compared, as well as the responses of PFC with reinforcement diameters of 0mm, 8mm, 16mm, and 24mm at the same speed. The specific conclusions are as follows:

C50 concrete demonstrates an impact load approximately four times greater than that of PFC at a velocity of 25 m/s. The energy absorption of PFC is approximately five times greater than that of C50 due to the fact that the failure mode of C50 is only a crack, whereas PFC exhibits full penetration at the same deformation.

After reinforcement, the peak load of PFC can increase by 15.2%. However, the reinforcement ratio has little effect on its peak load and energy dissipation. Therefore, reinforcement plays a crucial role in enhancing the strength and performance of PFC. Furthermore, the unreinforced PFC board experiences perforation failure, leading to energy dissipation that is 2.4 times higher than that of reinforced specimens.

In summary, higher concrete strength is associated with higher peak loads and greater energy absorption capacity, while reinforced bars have no significant effect on maximum impact load but enhance energy dissipation capacity relatively.PFC demonstrates significant potential as a high-performance construction material. This study analyzes the material's impact resistance which will generates a design framework for foam concrete components, while findings are valuable for advancing the development of foam concrete components.

REFERENCES

- Amrani, M., Taha, Y., Kchikach, A., 2020. Phosphogypsum recycling: New horizons for a more sustainable road material application. Journal of Building Engineering, 30, Pp. 101267.
- Cai, J., Ye, J., Wang, Y., 2017. Numerical study on dynamic response of reinforced concrete columns under low-speed horizontal impact loading. Procedia engineering, 210, Pp. 334-340.
- Calderón-Morales, B.R.S., García-Martínez, A., Pineda, P., 2021. Valorization of phosphogypsum in cement-based materials: Limits and potential in eco-efficient construction. Journal of Building Engineering, 44, Pp. 102506.
- Chernysh, Y., Yakhnenko, O., Chubur, V., 2021. Phosphogypsum recycling: a review of environmental issues, current trends, and prospects. Applied Sciences, 11 (4), Pp. 1575.
- Dancygier, A.N., Yankelevsky, D.Z., Jaegermann, C., 2007. Response of high performance concrete plates to impact of non-deforming projectiles. International Journal of Impact Engineering, 34 (11), Pp. 1768-1779.
- Gong, W.J., 2023. Numerical simulation study of dynamic response of reinforced concrete under diffe-rent impact loads. North Uniwersity of China.
- Lei, M., Liu, L., Lin, Y., 2020. Experimental investigation of damage evolution characteristics of C50 concrete under impact load. Shock and Vibration, Pp. 1-10.

- Li, J., Chang, J., Wang, T., 2022. Effects of phosphogypsum on hydration properties and strength of calcium aluminate cement. Construction and Building Materials, 347, Pp. 128398.
- Li, Y., Chen, J., Shi, S., Hu, L., Xu, X., 2023. Study of the design and flexural pe-rformance of an innovative fiber reinforced polymer/steel-concrete co-mposite beam. Advances in Structural Engineering, 26 (1), Pp. 121-
- Liu, S., Zhu, D., Li, G., 2018. Flexural response of basalt textile reinforce-d concrete with pre-tension and short fibers under low-velocity impact loads. Construction and Building Materials, 169, Pp. 859-876.
- Meskini, S., Samdi, A., Ejjaouani, H., 2021. Valorization of phosphogypsum as a road material: Stabilizing effect of fly ash and lime additives on strength and durability. Journal of Cleaner Production, 323, Pp. 129161.
- Peng, L., Yang, B., Deng, J., 2023. Study on the phosphogypsum proportion in foamed concrete based on concrete strength and carbon emission. Journal of Physics: Conference Series. IOP Publishing, 2510 (1), Pp. 012006.
- Pham, T.M., Wensu, C., Mohamed, E., 2021. Sensitivity of lateral impact response of RC columns reinforced with GFRP bars and stirrups to concrete strength and reinforcement ratio. Engineering Structures, Pp. 242.
- Pliaka, M., Gaidajis, G., 2022. Potential uses of phosphogypsum: A review. Journal of Environmental Science and Health, Part A, 57 (9), Pp. 746-763.
- Sadraie, H., Khaloo, A., Soltani, H., 2019. Dynamic performance of concrete slabs reinforced with steel and GFRP bars under impact loading. Engineering Structures, 191, Pp. 62-81.
- Tabatabaei, Z.S., Voiz, J.S., 2014. Comparative impact behavior of four lo-ng carbon fiber reinforced concretes. Materials and Design, 55, Pp. 212-223
- Wang, X.Y., 2023. Experiential study on the shear performance of high ductility recycled powder concrete beams. Shangdong Jianzhu University.
- Xiantao, Q., Yihu, C., Haowei, G., 2023. Resource utilization and development of phosphogypsum-based materials in civil engineering. Journal of Cleaner Production, Pp. 135858.
- Ye, Y.X., Hu, S.W., Yang, J.H., 2023. Impact resistance of reinforced concrete slabs under amplitude impacts. Journal of Harbin Institute of Technology, Pp. 1-12.
- Zineddin, M., Krauthammer, T., 2007. Dynamic response and behavior of reinforced concrete slabs under impact loading. International Journal of Impact Engineering, 34 (9), Pp. 1517-1534.

